Inorganic Chemistry

Article

pubs.acs.org/IC

Precise Electrochemical Control of Ferromagnetism in a Cyanide-Bridged Bimetallic Coordination Polymer

Yoshifumi Mizuno,[†,‡] Masashi Okubo,*[,†] Koichi Kagesawa,[†] Daisuke Asakura,[†] Tetsuichi Kudo,[†] Haoshen Zhou,*[,†] Katsuyoshi Oh-ishi,[‡] Atsushi Okazawa,[§] and Norimichi Kojima*[,§]

[†]National Institute of Advanced Industrial Science and Technology (AIST), Umezono 1-1-1, Tsukuba, Ibaraki 305-8568, Japan

[‡]Department of Applied Chemistry, Chuo University, Kasuga 1-13-27, Bunkyo-ku, Tokyo 112-8551, Japan

[§]Graduate School of Arts and Sciences, The University of Tokyo, Komaba 3-8-1, Meguro-ku, Tokyo 153-8902, Japan

Supporting Information

ABSTRACT: Magnetic coordination polymers can exhibit controllable magnetism by introducing responsiveness to external stimuli. This report describes the precise control of magnetism of a cyanide-bridged bimetallic coordination polymer (Prussian blue analogue: PBA) through use of an electrochemical quantitative Li ion titration technique, i.e., the galvanostatic intermittent titration technique (GITT). $K_{0.2}Ni[Fe(CN)_6]_{0.7}\cdot 4.7H_2O$ (NiFe-PBA) shows Li ion insertion/extraction reversibly accompanied with reversible Fe^{3+}/Fe^{2+} reduction/oxidation. When Li ion is inserted quantitatively into NiFe-PBA, the ferromagnetic transition temperature T_C gradually decreases due to reduction of paramagnetic Fe^{3+} to diamagnetic Fe^{2+}, and the ferromagnetic transition is completely suppressed for $Li_{0.6}$(NiFe-PBA). On the other hand, T_C increases continuously as Li ion is extracted due to oxidation of diamagnetic Fe^{2+} to paramagnetic Fe^{3+}, and the ferromagnetic transition is nearly recovered for Li_0(NiFe-PBA). Furthermore, the plots of T_C as a function of the amount of inserted/extracted Li ion x are well consistent with the theoretical values calculated by the molecular-field approximation.

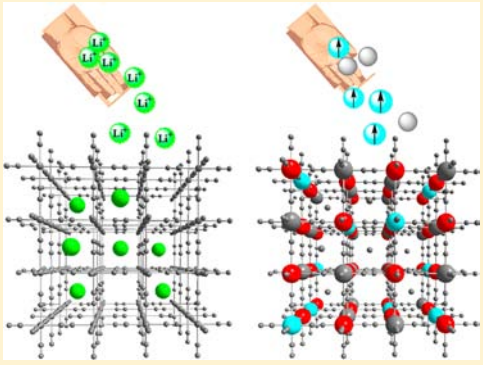

INTRODUCTION

Multifunctionality is an important concept in recent chemistry, because existence of multiple functionalities in a single phase can produce novel cooperative phenomena such as multiferroics.[1] In particular, coordination polymers possess potentially controllable electronic and structural properties; thus, they could provide a rational strategy achieving novel multifunctionalities.[2] For example, magnetic coordination polymers have been reported to show a wide variety of magnetic properties (e.g., room temperature ferrimagnetism,[3] spin-crossover,[4,5] Haldane gap[6]). In addition, other functionalities can also be introduced by designing the structure and electronic state. The coexistence of magnetism with another functionality frequently results in magnetism controllable by external stimuli (e.g., photoirradiation,[7−10] guest insertion,[11,12] and electric field application[13]), which can be applied to electronic switch devices. Therefore, controllable magnetism of coordination polymers has been investigated intensively.

Prussian blue analogue (PBA) is one of the best studied magnetic coordination polymers.[14] The cyanide-bridged perovskite-type structure of PBA generally is formulated as $A_{1-x}M[M'(CN)_6]_{1-y}\cdot\square_y\cdot nH_2O$ (A, alkali metal; M, M′, transition metal; □, $[M'(CN)_6]$ vacancy; hereafter denoted as MM′-PBA), and it possesses intriguing magnetism due to the strong σ and π donation/back-donation ability of the bridging cyanide ligand. Furthermore, the open porous structure of PBA permits the penetration of small guests, which could realize H_2 adsorption,[15] proton conduction,[16] ion exchange,[17] and ion storage.[18−23]

Recently, we have focused on the coexistence of magnetism and ion storage ability in PBA, and magnetism switching was achieved by electrochemical ion insertion/extraction. Bimetallic CuFe-PBA was switched reversibly between a ferromagnet and a paramagnet by galvanostatic solid state redox of the paramagnetic Fe^{3+}/diamagnetic Fe^{2+} couple.[24] Sato et al. also reported the electrochemical modification of magnetism of CrCr-,[25] FeFe-,[26] and NiFe-PBAs using a potentiostatic method.[27] However, these previous studies did not achieve precise control of the magnetism due to the difficulty in the quantitative ion/electron titration. To manipulate the electronic state and magnetism of PBA more quantitatively, an advanced electrochemical titration technique is required.

Here, we describe the precise electrochemical control of ferromagnetism of a bimetallic NiFe-PBA through use of a quantitative Li ion titration technique, i.e., the galvanostatic intermittent titration technique (GITT) (Scheme 1).

Received: June 26, 2012
Published: September 14, 2012

   dx.doi.org/10.1021/ic301361h | Inorg. Chem. 2012, 51, 10311−10316

Scheme 1. Schematic Illustration of Li Ion/Spin Distributions in the Coordination Polymer[a]

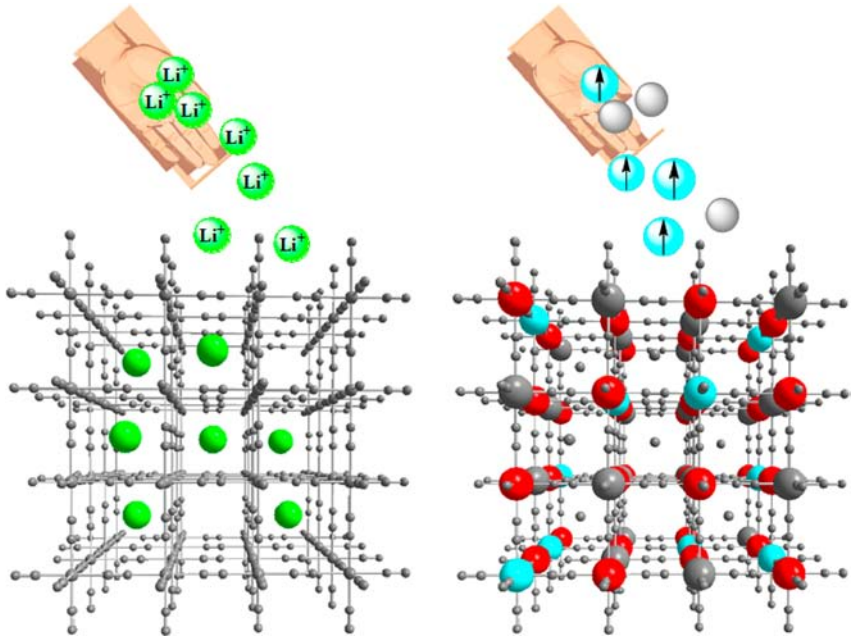

[a]The Li ions (green balls) are distributed in the porous space of the framework, while the magnetic low-spin Fe^{3+} (cyan balls) and diamagnetic low-spin Fe^{2+} (gray balls) are distributed on the host framework with the fixed magnetic Ni^{2+} (red balls).

EXPERIMENTAL SECTION

NiFe-PBA was synthesized by a precipitation method. An aqueous solution of 0.15 M $NiCl_2{\cdot}6H_2O$ was added dropwise to an aqueous solution of 0.1 M $K_3Fe(CN)_6$. The precipitate was centrifuged, washed with distilled water, and then dried in vacuo for 24 h. The obtained products were stored under an inert atmosphere in the dark at 5 °C to prevent decomposition.

The composition was determined by the standard microanalytical method for C, H, and N elements and coupled plasma mass spectroscopy for K, Fe, and Ni elements. Calcd for $K_{0.2}Ni[Fe(CN)_6]_{0.7}{\cdot}4.7H_2O$: K, 2.61; Ni, 19.6; Fe, 13.1; C, 16.84; N, 19.64; H, 3.16. Found: K, 2.16; Ni, 20.1; Fe, 13.3; C, 16.60; N, 18.96; H, 3.04.

Powder X-ray diffraction (XRD) measurement was carried out on a Bruker D8 Advance using Cu Kα radiation in steps of 0.01° over the 2θ range of 5−80°. The unit cell parameters were calculated by least-squares fitting with peak top values.

For the electrochemical Li ion insertion/extraction, three electrode glass cells were used. NiFe-PBA was ground with 20 wt % acetylene black and 5 wt % poly(tetrafluoroethylene) into a paste and used as the working electrode. For the counter and reference electrode, Li metal was used. For the electrolyte, 1 M $LiClO_4$/ethylene carbonate−diethyl carbonate (EC−DEC, 1:1 V/V %) was used. The cutoff voltages were 2.0 and 4.3 V (vs Li/Li^+).

The direct current (DC) magnetic susceptibility was measured on a Quantum Design MPMS5S SQUID susceptometer. The magnetic susceptibility was corrected for core diamagnetism estimated from Pascal's constants and Pauli paramagnetism because of the used acetylene black and icosane. For ^{57}Fe Mössbauer spectroscopy, ^{57}Co in Rh was used as Mössbauer source. The spectra were calibrated by using six lines of α-Fe, the center of which was taken as zero isomer shifts.

RESULTS AND DISCUSSION

NiFe-PBA was synthesized by a precipitation method. Figure 1 shows the powder X-ray diffraction pattern for NiFe-PBA. The XRD pattern indicated a single cubic phase without crystalline impurity. The estimated unit cell parameters were a = 10.204(3) Å and V = 1062(1) $Å^3$. These values are well consistent with the previously reported values (a = 10.229(5) Å).[28] The precise composition was determined as $K_{0.2}Ni[Fe^{2+}(CN)_6]_{0.1}[Fe^{3+}(CN)_6]_{0.6}{\cdot}\square_{0.3}{\cdot}4.7H_2O$ based on the standard microanalytical method (C, H, and N) and coupled plasma mass spectroscopy (K, Fe, and Ni). The existence of $[Fe^{2+}(CN)_6]$ in NiFe-PBA was clearly suggested by the ^{57}Fe Mössbauer spectrum, and the amount of $[Fe^{2+}(CN)_6]$ was confirmed from the amount of electrochemically inserted Li ion (see below).

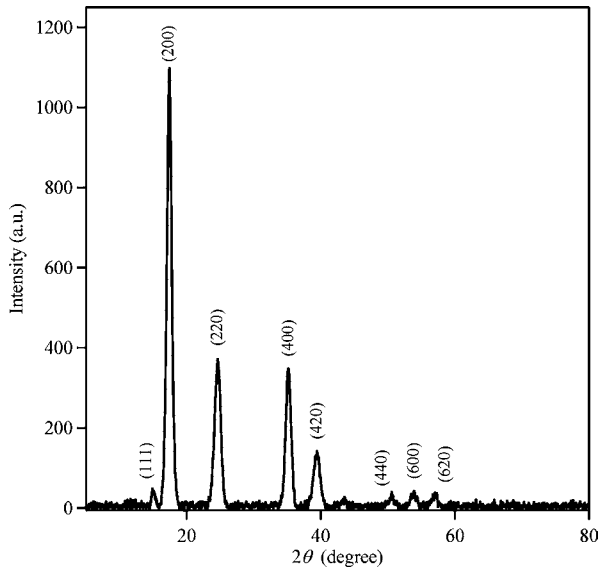

Figure 1. Powder X-ray diffraction pattern for NiFe-PBA.

Electrochemical Li ion insertion/extraction reaction was conducted for NiFe-PBA. Figure 2 shows the cyclic voltammogram (CV) at a scan rate of 0.1 $mV{\cdot}s^{-1}$. A cathodic peak was observed at 3.22 V, while an anodic peak was observed at 3.43 V. According to previous reports, these peaks could be ascribed to the Li ion insertion and extraction, respectively, accom-

dx.doi.org/10.1021/ic301361h | Inorg. Chem. 2012, 51, 10311−10316

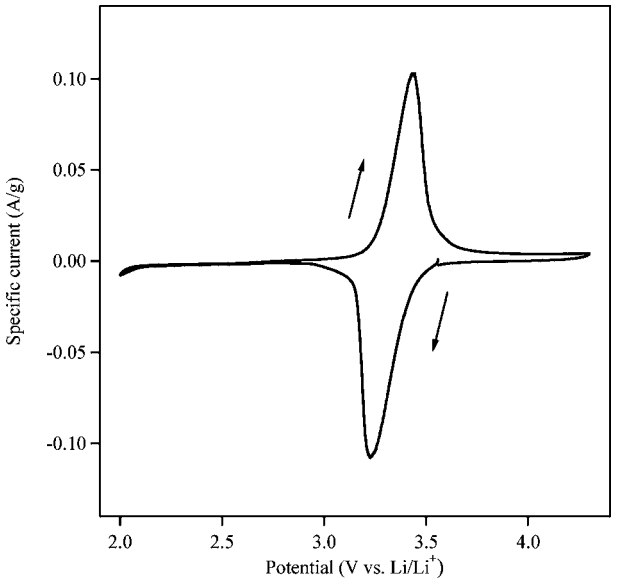

Figure 2. Cyclic voltammogram for NiFe-PBA in 1 M $LiClO_4$/EC-DEC electrolyte. Scan rate was 0.1 mV/s.

panied by the solid-state redox of $[Fe^{3+}(CN)_6]/[Fe^{2+}(CN)_6]$ couple in NiFe-PBA.[18−23] The electrochemical reaction of NiFe-PBA can be described as

$$x\mathrm{Li}^+ + x\mathrm{e}^- + \mathrm{NiFe}^{3+}\text{-PBA} \leftrightarrow \mathrm{Li}_x(\mathrm{NiFe}^{2+}{}_x\mathrm{Fe}^{3+}{}_{1-x}\text{-PBA})$$

However, controlled potential methods such as CV could not determine the true equilibrium potential of the material, and performing the quantitative Li ion titration into NiFe-PBA was also difficult. Therefore, an advanced electrochemical characterization, i.e., the galvanostatic intermittent titration technique (GITT),[29] was performed. In the GITT experiment, a low-density constant current (current density; 18 mA/g) was repeatedly applied for 10 min, followed by interruption for 30 min to obtain the open circuit voltage (OCV) at each equilibrium state (Figure 3a). The open triangles in Figure 3b show the OCVs as a function of x in Li_x(NiFe-PBA). The amount of inserted/extracted Li ion x was calculated based on Faraday's law.[30] The OCVs showed that 0.6 Li ion could be inserted/extracted reversibly ($0 < x < 0.6$ for Li_x(NiFe-PBA)) at the potential range between 3.4 and 3.2 V vs Li/Li^+. The observed potential plateaus agreed well with the redox peaks recorded in the CV.

The ex situ XRD patterns were measured for Li_x(NiFe-PBA) ($0 < x < 0.6$) to clarify structural changes occurring during the quantitative Li ion insertion/extraction (Figure 4a). During Li ion insertion/extraction, all of the peaks shifted gradually without emergence of an additional peak, suggesting that the Li ion insertion proceeded via a solid solution process. The lattice constant is plotted as a function of x in Figure 4c (closed triangles). Li ion insertion/extraction of the NiFe-PBA framework resulted in a slight shrinkage of the lattice constant from 10.25 Å ($x = 0$) to 10.199 Å ($x = 0.6$) and a slight expansion of that from 10.199 Å ($x = 0.6$) to 10.24 Å ($x = 0$). This result confirms the reversible lattice shrinkage/expansion during Li ion insertion/extraction. Furthermore, the lattice constant changed linearly during Li ion insertion/extraction, which is consistent with Vegard's law commonly observed for binary alloys.[31] Therefore, these results confirm the solid

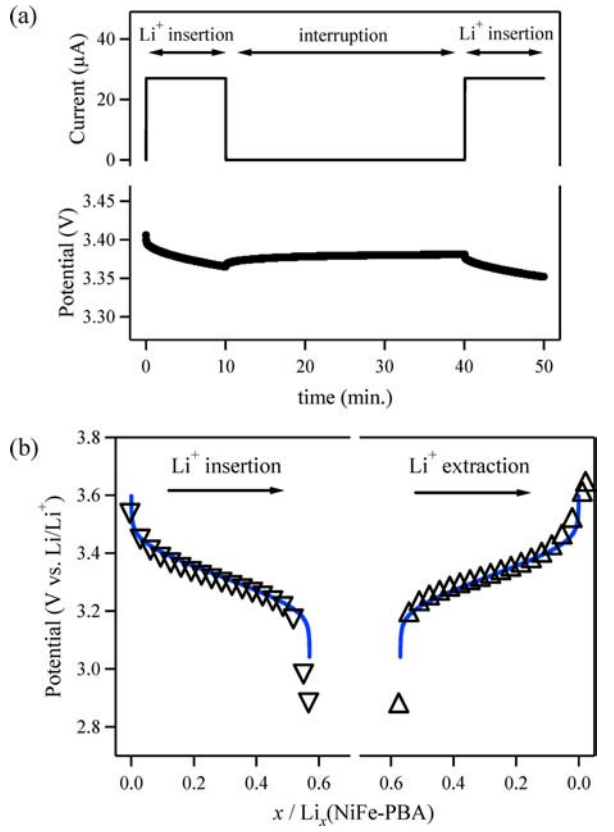

Figure 3. (a) Time dependence of potential and current during the GITT. (b) Open circuit voltage (open triangles) for Li_x(NiFe-PBA) during Li ion insertion/extraction. Blue lines are theoretical curves based on the mean-field approximation.

solution state of the entire composition Li_x(NiFe-PBA) ($0 < x < 0.6$).

To clarify the change in the electronic structure, ^{57}Fe Mössbauer spectra were recorded during Li ion insertion/extraction (Figure 4b). The filled dots in Figure 4b are experimental data, and broken lines are fitted curves. All of the spectra could be fitted successfully using a combination of a low-spin Fe^{3+} doublet and a low-spin Fe^{2+} singlet (Figure 4b and Table S1 in the Supporting Information).[32] Before Li ion insertion, the spectrum for NiFe-PBA was fitted with a main doublet of Fe^{3+} low-spin and a small singlet of Fe^{2+} low-spin. This result supports the existence of $[Fe^{2+}(CN)_6]$ in as-prepared NiFe-PBA. During Li ion insertion, Fe^{3+} in Li_x(NiFe-PBA) was continuously reduced to Fe^{2+}. Almost a half of Fe^{3+} was reduced to Fe^{2+} for $Li_{0.3}$(NiFe-PBA), and then Fe^{3+} was completely reduced to Fe^{2+} for $Li_{0.6}$(NiFe-PBA). Fe^{2+} was gradually oxidized to Fe^{3+} during Li ion extraction. In the case of $Li_{0.3}$(NiFe-PBA) during Li ion extraction, 40% of Fe^{2+} was oxidized to Fe^{3+}, while Fe^{2+} was almost completely oxidized (89.4%) to Fe^{3+} for Li_0(NiFe-PBA) after Li ion extraction. These results confirmed that the reversible Fe^{3+}/Fe^{2+} reduction/oxidation occurred during Li ion insertion/extraction. The Fe^{3+} fraction in Li_x(NiFe-PBA) during Li ion insertion/extraction changed linearly as a function of x (open circles in Figure 4c). Therefore, the precise and quantitative titration of the Li ion and electron pair was achieved by GITT.

In general, when the guest Li ions are distributed in the host, the free energy of the system can be described by the lattice-gas model.[33] In particular, as long as the nearest neighboring Li^+−

dx.doi.org/10.1021/ic301361h | Inorg. Chem. 2012, 51, 10311−10316

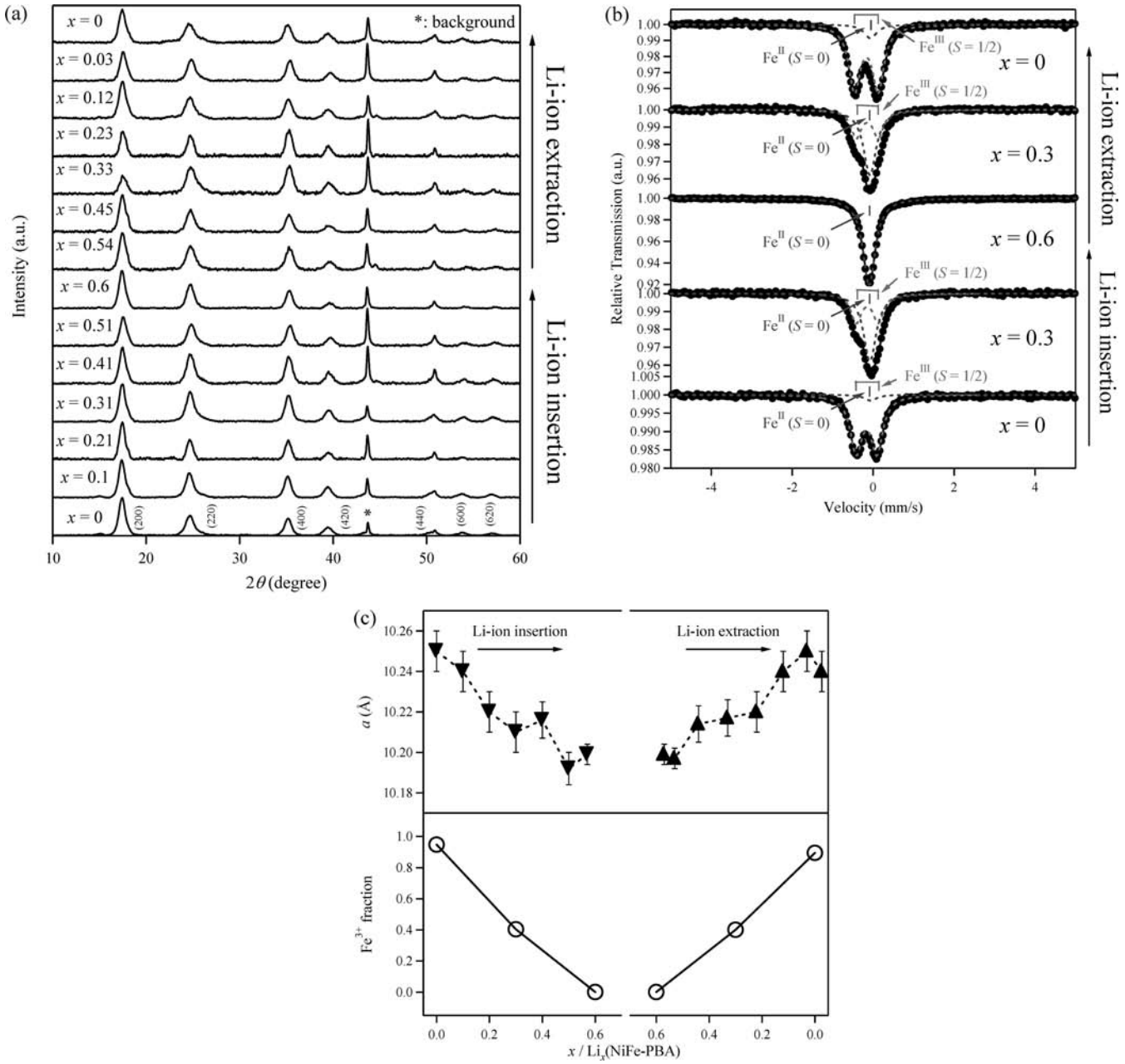

Figure 4. (a) Ex situ XRD patterns for Li_x(NiFe-PBA) during Li ion insertion/extraction (*: background). (b) ^{57}Fe Mössbauer spectra for Li_x(NiFe-PBA) during Li ion insertion/extraction (closed dots, experimental data; broken lines, fitted curves). (c) Lattice constant (closed triangles) and Fe^{3+} fraction (opened circles) as a function of x in Li_x(NiFe-PBA).

Li^+ interaction J_{Li} is assumed to be weak, the system can be treated by the mean field approximation.[30] Based on this approximation, the OCV curve for Li_x(NiFe-PBA) is given as

$$E(x) = E_0 + \frac{zJ_{Li}}{F}\frac{x}{x_0} - \frac{RT}{F}\ln\left(\frac{x}{x_0 - x}\right)$$

Here, E_0 is the formal potential, z is the number of the nearest neighbor Li ion sites, and x_0 is the maximum of x. The blue line in Figure 3b is the fitted results with E_0 = 3.39 V and J_{Li} = −12 meV/mol. The expression reproduced the experimental OCV, which indicates that the model is appropriate for description of the Li ion distribution in NiFe-PBA. The small negative J_{Li} suggests weak repulsion between the neighboring Li ions due to Coulombic interaction.

The above results demonstrated the quantitative Li ion titration in NiFe-PBA, in which the valence state of Fe was quantitatively controlled between the paramagnetic $[Fe^{3+}(CN)_6]^{3-}$ and diamagnetic $[Fe^{2+}(CN)_6]^{4-}$. Therefore, the magnetic measurements were conducted for Li_x(NiFe-PBA) during Li ion insertion/extraction to clarify the magnetic properties.

Li_0(NiFe-PBA) had a χT value of 2.01 emu·K·mol^{-1} at room temperature, which is greater than the spin-only value (1.23 emu·K·mol^{-1}). This difference can be ascribed partly to contribution from the orbital angular momentum of low-spin Fe^{3+} ions. Furthermore, although the XRD pattern for NiFe-PBA indicated a single cubic phase without crystalline impurity, the amorphous magnetic impurities, which cannot be detected in the XRD experiments, could also contribute to the large χT

dx.doi.org/10.1021/ic301361h | Inorg. Chem. 2012, 51, 10311−10316

value. With decreasing temperature T, χT increased monotonically with a Weiss constant θ of 23.7 K (Figure S1a in the Supporting Information). This result indicates ferromagnetic interaction between Fe^{3+} and Ni^{2+}. The black open triangles in Figure 5a are the field-cooled magnetization M_{FC} of Li_0(NiFe-PBA) under 10 Oe. The zero-field and remnant magnetizations are showed in Figure S2a in the Supporting Information. The drastic increase in M_{FC} below 27 K suggests a ferromagnetic transition. The Curie temperature T_C estimated from the peak-top temperature of dM_{FC}/dT plots (black closed triangles in Figure 5a) is 22.4 K, which is similar to the previously reported value (23.6 K).[28]

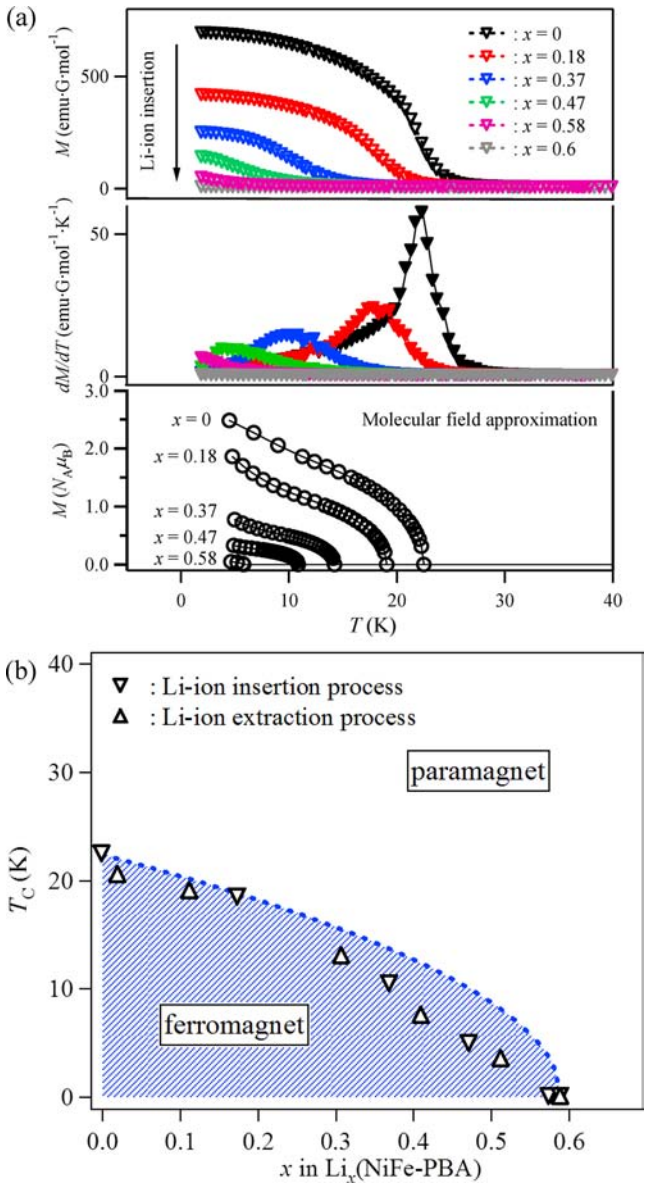

Figure 5. (a) Field cooled magnetization M_{FC} (opened triangles), dM_{FC}/dT (closed triangles), and calculated spontaneous magnetization (open circles) for Li_x(NiFe-PBA). J_{spin} = 5.9 K was used in the calculation (see text). (b) $x-T_C$ phase diagram of Li_x(NiFe-PBA). Blue dotted line is the theoretical curve based on the mean-field approximation (see text).

Upon insertion of Li ion, χT at room temperature decreased continuously from 2.01 (x = 0) to 1.18 emu·K·mol^{-1} (x = 0.6). The χT value for $Li_{0.6}$(NiFe-PBA) did not show temperature dependence (Figure S1a in the Supporting Information), suggesting the disappearance of the ferromagnetic interaction between Fe^{3+} and Ni^{2+}. The open triangles in Figure 5a are M_{FC} of Li_x(NiFe-PBA) (x = 0.18, 0.37, 0.47, 0.58, and 0.6) under 10 Oe. The onset temperature exhibiting a drastic increase in M_{FC} was reduced continuously with increasing x. The T_C value estimated from the dM_{FC}/dT plot (closed triangles in Figure 5a) decreased from 22.4 K (x = 0) to 0 K (x = 0.6). In fact, $Li_{0.6}$(NiFe-PBA) showed no clear peak in the dM_{FC}/dT plot. These results suggest that the ferromagnetic transition was completely suppressed by 0.6 Li ion insertion, because the reduction of paramagnetic Fe^{3+} to diamagnetic Fe^{2+} eliminated the ferromagnetic interaction between the nearest neighboring spins.

In contrast, when Li ion was extracted from $Li_{0.6}$(NiFe-PBA), χT at room temperature increased continuously from 1.18 (x = 0.6) to 2.24 emu·K·mol^{-1} (x = 0 after Li ion extraction). The Weiss constant of Li_0(NiFe-PBA) after Li ion extraction is 20.6 K. This value suggests a recovered ferromagnetic interaction between Fe^{3+} and Ni^{2+} during reversible Li ion insertion/extraction. The onset temperature exhibiting a drastic increase in M_{FC} increased continuously with decreasing x, and T_C estimated from the dM_{FC}/dT plot increased from 0 K (x = 0.6) to 20.8 K (x = 0 after Li ion extraction) (Figure S3 in the Supporting Information). Although T_C for Li_0(NiFe-PBA) after Li ion extraction was slightly lower than that for NiFe-PBA before Li ion insertion due to the slight increment of diamagnetic Fe^{2+}, the ferromagnetic transition was nearly recovered after Li ion extraction.

The M_{FC} vs T plot showed the systematic control of T_C by x. In general, if the electron is distributed randomly on the Fe ions of the NiFe-PBA lattice, the free energy of the magnetic system can again be described by the mean-field approximation (so-called the molecular field approximation for the magnetic system).[34] The Hamiltonian for Li_x(NiFe-PBA) without external field can be described by

$$H = -2z_{Fe}J_{spin}\langle S_{Fe}\rangle\sum \mathbf{S}_{Ni} - 2z_{Ni}J_{spin}\langle S_{Ni}\rangle\sum \mathbf{S}_{Fe}$$

where z_i is the number of the nearest neighboring spin i (z_{Fe} = $6(0.6 - x)$ and z_{Ni} = 6), J_{spin} is the superexchange constant between Fe^{3+} and Ni^{2+}, and $\langle S_i\rangle$ is the averaged value of the spin i. This can provide the temperature dependence of the spontaneous magnetization and T_C for various x. The open circles in Figure 5a depict the numerically calculated temperature dependence of the spontaneous magnetization M for various x. Note that J_{spin} was assumed to be constant (5.9 K) regardless of x. The calculated M vs T plots for various x showed that the increase in x reduced both the onset temperature of M and the M value at low temperatures. The calculated plots reproduced the temperature dependence of experimental M_{FC}.

To further validate the molecular-field model, the $x-T$ phase diagram for Li_x(NiFe-PBA) was plotted (Figure 5b). The open triangles are T_C estimated from the dM/dT plots for Li_x(NiFe-PBA) during Li ion insertion (∇)/extraction (Δ), respectively. The molecular-field approximation provides the x-dependence of T_C for Li_x(NiFe-PBA) as $T_C(x) = [1 - (x/0.6)]^{1/2}T_C(x=0)$, which is shown as a broken blue line in Figure 5b. The estimated T_C values were almost consistent with the theoretical plot, which confirmed the random distribution of the inserted spin.

dx.doi.org/10.1021/ic301361h | Inorg. Chem. 2012, 51, 10311−10316

CONCLUSIONS

The precise control of ferromagnetism of NiFe-PBA was achieved by electrochemical quantitative Li ion/spin titration. 0.6 Li ion could insert/extract into NiFe-PBA reversibly ($0 < x < 0.6$). The reversible lattice shrinkage/expansion in NiFe-PBA during Li ion insertion/extraction suggested the solid solution process for the entire composition. The ^{57}Fe Mössbauer spectra showed the reversible solid state redox of the paramagnetic Fe^{3+}/diamagnetic Fe^{2+} couple. Therefore, when Li ion inserted quantitatively, T_C of NiFe-PBA decreased gradually, and the ferromagnetic transition is completely suppressed for $x = 0.6$. On the other hand, T_C increased gradually as Li ion is extracted. Thus, the ferromagnetism of NiFe-PBA was manipulated quantitatively by an advanced electrochemical titration technique. Furthermore, both the inserted Li ions and spins were distributed randomly in NiFe-PBA, which was confirmed by fitting the experimental results to the corresponding thermodynamic functions based on the mean-field approximation.

ASSOCIATED CONTENT

Supporting Information

GITT measurements, Mössbauer parameters, and additional magnetic data. This material is available free of charge via the Internet at http://pubs.acs.org.

AUTHOR INFORMATION

Corresponding Author

*Tel: +81 (0)29 861 3489. Fax: +81 (0)29 3489. E-mail: m-okubo@aist.go.jp, h.s.zhou@aist.go.jp, cnori@mail.ecc.u-tokyo.ac.jp.

Author Contributions

Y.M., M.O., D.A., T.K., H.Z., and K.O. analyzed results of electrochemical measurements. Y.M., M.O., K.K., A.O., and N.K. analyzed results of magnetic measurements. All authors discussed the results and commented on the manuscript.

Notes

The authors declare no competing financial interest.

ACKNOWLEDGMENTS

This work was financially supported by Industrial Technology Research Grant Program in 2010 from New Energy and Industrial Development Organization (NEDO).

REFERENCES

(1) Hwang, H. Y.; Iwasa, Y.; Kawasaki, M.; Keimer, B.; Nagaosa, N.; Tokura, Y. *Nat. Mater.* **2012**, *11*, 103−113.
(2) Zhou, H.-C.; Long, J. R.; Yaghi, O. M. *Chem. Rev.* **2012**, *112*, 673−674.
(3) Ferlay, S.; Mallah, T.; Ouahes, R.; Veillet, P.; Verdaguer, M. *Nature* **1995**, *378*, 701−703.
(4) Kondo, A.; Kajiro, H.; Noguchi, H.; Carlucci, L.; Proserpio, D. M.; Ciami, G.; Kato, K.; Taketa, M.; Seki, H.; Sakamoto, M.; Hattori, Y.; Okino, F.; Maeda, K.; Ohba, T.; Kaneko, K.; Kanoh, H. *J. Am. Chem. Soc.* **2011**, *133*, 10512−10522.
(5) Bhar, K.; Khan, S.; Costa, J. S.; Ribas, J.; Roubeau, O.; Mitra, P.; Ghosh, B. K. *Angew. Chem., Int. Ed.* **2012**, *51*, 2142−2145.
(6) Renard, J. P.; Verdaguer, M.; Regnault, L. P.; Erkelens, W. A. C.; Rossatmignod, J.; Ribas, J.; Stirling, W. G.; Vettier, C. *J. Appl. Phys.* **1988**, *63*, 3538−3541.
(7) Sato, O.; Iyoda, T.; Fujishima, A.; Hashimoto, K. *Science* **1996**, *272*, 704−706.
(8) Neville, S. M.; Halder, G. J.; Chapman, K. W.; Duriska, M. B.; Southon, P. D.; Cashion, J. D.; Létard, J.-F.; Moubaraki, B.; Murray, K. S.; Kepert, C. J. *J. Am. Chem. Soc.* **2008**, *130*, 2869−2876.
(9) Kida, N.; Hikita, M.; Kashima, I.; Okubo, M.; Itoi, M.; Enomoto, M.; Kato, K.; Takara, M.; Kojima, N. *J. Am. Chem. Soc.* **2009**, *131*, 212−220.
(10) Ohkoshi, S.; Imoto, K.; Tsunobuchi, Y.; Takano, S.; Tokoro, H. *Nat. Chem.* **2011**, *3*, 564−569.
(11) Agustí, G.; Ohtani, R.; Yoneda, K.; Gaspar, A. B.; Ohba, M.; Sánchez-Royo, J. F.; Muñoz, M. C.; Kitagawa, S.; Real, J. A. *Angew. Chem., Int. Ed.* **2009**, *48*, 8944−8947.
(12) Ohtani, R.; Yoneda, K.; Furukawa, S.; Horike, N.; Kitagawa, S.; Gasper, A. B.; Muñoz, M. C.; Real, J. A.; Ohba, M. *J. Am. Chem. Soc.* **2011**, *138*, 8600−8605.
(13) Mahfoud, T.; Molnár, G.; Bonhommeau, S.; Cobo, S.; Salmon, L.; Demont, P.; Tokoro, H.; Ohkoshi, S.; Boukheddaden, K.; Bousseksou, A. *J. Am. Chem. Soc.* **2009**, *131*, 15049−15054.
(14) Miller, J. S.; Drillon, M. *Molecules to Materials*, 5th ed.; Wiley-VCH Verlag GmbH & Co.: 2005.
(15) Kaye, S. S.; Long, J. R. *J. Am. Chem. Soc.* **2005**, *127*, 6506−6507.
(16) Ohkoshi, S.; Nakagawa, K.; Tomono, K.; Imoto, K.; Tsunobuchi, Y.; Tokoro, H. *J. Am. Chem. Soc.* **2010**, *132*, 6620−6621.
(17) Matsuda, T.; Kim, J.; Moritomo, Y. *J. Am. Chem. Soc.* **2010**, *132*, 12206−12207.
(18) Itaya, K.; Ataka, T.; Toshima, S. *J. Am. Chem. Soc.* **1982**, *104*, 4767−4772.
(19) Imanishi, N.; Morikawa, T.; Kondo, J.; Takeda, Y.; Yamamoto, O.; Kinugasa, N.; Yamagishi, T. *J. Power Sources* **1999**, *79*, 215−219.
(20) Okubo, M.; Asakura, D.; Mizuno, Y.; Kim, J.-D.; Kudo, T.; Honma, I. *J. Phys. Chem. Lett.* **2010**, *1*, 2063−2071.
(21) Asakura, D.; Okubo, M.; Mizuno, Y.; Kudo, T.; Zhou, H.; Amemiya, K.; de Groot, F. M. F.; Chen, J.-L.; Wang, W.-C.; Glans, P.-A.; Chang, C.; Guo, J.; Honma, I. *Phys. Rev. B* **2011**, *84*, 045117.
(22) Mizuno, Y.; Okubo, M.; Asakura, D.; Saito, T.; Hosono, E.; Saito, Y.; Oh-ishi, K.; Kudo, T.; Zhou, H. *Electrochim. Acta* **2012**, *63*, 139−145.
(23) Asakura, D.; Okubo, M.; Mizuno, Y.; Kudo, T.; Zhou, H.; Ikedo, K.; Mizokawa, T.; Okazawa, A.; Kojima, N. *J. Phys. Chem. C* **2012**, *116*, 8364−8369.
(24) Okubo, M.; Asakura, D.; Mizuno, Y.; Kudo, T.; Zhou, H.; Okazawa, A.; Kojima, N.; Ikedo, K.; Mizokawa, T.; Honma, I. *Angew. Chem., Int. Ed.* **2011**, *50*, 6269−6274.
(25) Sato, O.; Iyoda, T.; Fujishima, A.; Hashimoto, K. *Science* **1996**, *271*, 49−51.
(26) Sato, O.; Hayami, S.; Einaga, Y.; Gu, Z.-Z. *Bull. Chem. Soc. Jpn.* **2003**, *76*, 443−470.
(27) Sato, O. *J. Solid State Electrochem.* **2007**, *11*, 773−779.
(28) Juszczyk, S.; Johansson, C.; Hanson, M.; Ratuszna, A.; Małecki, G. *J. Phys.: Condens. Matter* **1994**, *6*, 5697−5706.
(29) Weppner, W.; Huggins, R. A. *J. Electrochem. Soc.* **1977**, *124*, 1569−1578.
(30) Bard, A. J.; Faulkner, L. R. *Electrochemical Methods: Fundamentals and Application*, 2nd ed.; John Wiley & Sons, Inc.: 2001.
(31) Christian, J. W. *The Theory of Transformations in Metals and Alloys*, 3rd ed.; Elsevier Science Ltd.: 2002.
(32) Greenwood, N. N.; Gibb, T. C. *Moessbauer Spectroscopy*; Chapman & Hall: London, 1971.
(33) Bruce, P. G. *Solid State Electrochemistry*; Cambridge University Press: 1995.
(34) Blundell, S. *Magnetism in Condensed Matter*; Oxford University Press: 2001.